Investigating channel flow using wall shear stress signals at transitional Reynolds numbers

Rishav Agrawal, Henry C.-H. Ng, David J. C. Dennis, Robert J. Poole*

School of Engineering, University of Liverpool, Liverpool L69 3GH, UK

Abstract

Time-resolved wall shear stress measurements are conducted to investigate channel flow at transitional Reynolds numbers. Constant temperature anemometry (CTA) is employed to measure the instantaneous wall shear stress using glue-on hot films as the sensing probes. Pressure-drop measurements are conducted to calibrate the mean hot-film voltage signals and to ensure that the pressure drop is measured in the so-called "fully-developed" region of the channel, a study of effect of entrance length on the pressure-drop measurements is carried out. Time history and higher order statistics of wall shear stress fluctuations reveal that the flow remains laminar until $Re_\tau(= u_\tau h/\nu) \approx 43$ in our channel flow facility, where u_τ, h and ν are the friction velocity, channel half-height and kinematic viscosity, respectively. Third and fourth order moments of wall shear stress jump at the onset of transition and increase significantly until they reach maxima at about $Re_\tau \approx 48$. After this Reynolds number, these two higher order moments start to decrease gradually with increasing Reynolds number and after $Re_\tau \approx 73-79$, any significant dependence of these two moments on Reynolds number disappears. Multiple hot-film measurements, which are located at different spatial locations, are conducted to characterize the large-scale turbulent structures. It is observed that there are structures, at least $7h$ wide, for Re_τ between 46.8 and 53.9. Two-point spatial correlations reveal that on average these large structures are angled at approximately 17^o for $Re_\tau = 46.8$ and roughly between 32^o and 37^o for $48.7 < Re_\tau < 53.9$ relative to the streamwise direction.

Keywords: Transition to turbulence, hot-film anemometry

1. Introduction

The transition to turbulence in shear flows has remained an active topic of investigation in fluid mechanics since the classical experimental work of Osborne Reynolds in the 19th century (Reynolds, 1883). In addition to its significance in fundamental research, understanding transition phenomenon is also useful for many practical applications. For example, turbulent flow provides better mixing and heat transfer than laminar flow and therefore understanding the transition phenomenon may help in more efficient designs for mixing and heat transfer applications. There are also many situations where the flow is required to remain in a laminar state to reduce the skin friction drag. For all these applications, it is necessary to have a better understanding of the transition process. But still, transition is one of the least understood areas of fluid mechanics due to the complex spatiotemporal nature of the flow during transition. The present study focusses on the transition in a planar channel flow, which comes under the class of canonical wall-bounded flows.

In planar channel flows, laminar flow is found to be unstable and can enter into the turbulent state well below the critical Reynolds number of linear stability (Orszag, 1971), if finite amplitude disturbances are present (Patel & Head, 1969; Carlson et al., 1982; Alavyoon et al., 1986; Sano & Tamai, 2016). Various past experiments and numerical simulations have found this subcritical transition to be related to the large localized coherent structures observed called turbulent spots (Carlson et al., 1982; Alavyoon et al., 1986; Sano & Tamai, 2016; Aida et al., 2010). In early experiments, using flow visualization in a channel flow, Carlson et al. (1982) and Alavyoon et al. (1986) observed that these turbulent spots grow as they flow downstream with their leading edge propagating at a higher speed than the trailing edge. Lemoult et al. (2013) used particle image velocimetry (PIV) to investigate the formation and growth of a turbulent spot in a plane Poiseuille flow (PPF). They used a channel flow facility of an aspect ratio (AR) of $w/2h = 7.5$ and showed that the flow region around the spot can be divided into two scales: large-scale ($> 5h$) and small-scale ($< 5h$), where w and h indicate channel width and half-height respectively. In the present study, to study the large-scale coherent structures during transition, the same definition for large-scale is employed. These turbulent spots, which originate at the onset of transition, have been shown to develop into stripes with increasing Reynolds numbers by Aida et al. (2010). Tsukahara et al. (2005) carried out direct numerical simulations (DNS) for channel flow at Reynolds number $830 \leq Re_h \leq 2865$ by using different computational domain sizes, where $Re_h = U_b h/\nu$ and U_b, h and ν indicate bulk velocity, channel half-height and kinematic viscosity of the fluid, respectively. The largest computational domain had a dimension of $L_x \times L_z = 51.2h \times 22.5h$, where x and z represent streamwise and spanwise directions, respectively. They applied a periodic boundary condition in the streamwise and spanwise directions and a no-slip condition on

*Corresponding author

Email address: robpoole@liverpool.ac.uk (Robert J. Poole)

the top and bottom walls. They observed the presence of a periodic weak-turbulence region for $Re_h (Re_\tau = u_\tau h/\nu) = 1160(80)$ which looked similar to puff-like structures observed in transitional pipe flows (Wygnanski & Champagne, 1973; Wygnanski et al., 1975). Here, u_τ indicates the friction velocity. These periodic weak-turbulence structures were found to be inclined with the streamwise direction at an angle of about 24°. Brethouwer et al. (2012) conducted DNS in a channel flow of domain size $L_x \times L_z = 55h \times 25h$ for $Re_h = 933$, and observed similar puff-like structures. Tuckerman et al. (2014) carried out DNS in a channel flow of domain size $L_x \times L_z = 10h \times 40h$, where the computational domain was tilted at 24° with respect to the mean flow direction. They observed turbulent-laminar bands, similar to those observed by Tsukahara et al. (2005), for $Re_h = 1100$ at an angle of 24° with the mean flow direction. Using flow visualization in a channel, Tsukahara et al. (2014) found turbulent stripes for Re_h between 850 and 1000. These stripy structures were observed to consist of laminar and turbulent regions, and inclined at an angle of 20°-30° with the streamwise direction. Using direct numerical simulation (DNS), Aida et al. (2014) investigated the growth of a single turbulent spot and observed the presence of "stripy" structures inside the spots which contain so-called quasi-laminar and turbulent regions.

Pomeau (1986) conjectured that the transition to turbulence is potentially related to the directed percolation (DP) university class. This conjecture was based on the idea that the intermittent nature of transition in wall-bounded flows can be modelled using DP theory. DP is a class of non-equilibrium phase transitions which can be used to explain different stochastic spreading processes. The DP universality class has a characteristic set of critical exponents which usually depend on the spatial dimension (D) of the physical process. Many physical processes such as wildfires, epidemics and flow through a porous media are found to be potentially related to this class. Further literature on the relevance of the DP universality class on different physical processes can be found in Hinrichsen (2000), Takeuchi et al. (2007) and Henkel et al. (2008). Recently, Sano & Tamai (2016) attempted to observe the analogy between the transition to turbulence in channel flows and DP univesality class. They carried out an experimental investigation of transition in a channel flow facility using a flow visualization technique. They injected perturbations at the inlet which either decayed or spread depending on the Reynolds number. Close to the onset of transition, the critical exponents were found to be similar to the (2+1)D DP universality class. This suggested that the transition to turbulence in channel flows is related to the (2+1)D DP universality class. This observation suggests that the spatiotemporal intermittency, which is generally observed in the laminar-turbulent transition in wall-bounded flows, belongs to the DP universality class. The relationship between DP and laminar-turbulent transition is also shown in the same journal issue for Taylor-Couette flow by Lemoult et al. (2016). Xiong et al. (2015) carried out DNS in a channel flow at transitional Reynolds numbers using as in other studies periodic boundary conditions in the streamwise and spanwise directions, and no-slip boundary conditions on the wall. The computational domain was larger than those earlier studies and had a size of $L_x \times L_z = 160h \times 120h$. It was seen that localized perturbations evolve into oblique turbulent bands beyond $Re_h = 660$. However these bands break and decay due to interaction with other turbulent bands and localized perturbations for lower Reynolds number. Only for $Re_h \geq 1000$, did these turbulent bands give rise to sustained turbulence. Tao et al. (2018) conducted DNS of channel flow using similar boundary conditions as used by Xiong et al. (2015), and observed the presence of sparse oblique turbulent bands near the onset of transition. They employed different sizes of the computational domains to investigate the dependency of the band growth and breaking on size of the computational domain. They found that these sparse bands can lead to very small values of turbulence fraction in an arbitrarily large flow domain. Chantry et al. (2017) also discuss domain size issues by carrying out numerical investigation in a so-called Waleffe flow of computational domain as large as $L_x \times L_z = 2560h \times 2560h$. A good agreement with the (2+1)D DP universality class was obtained which they attributed to the presence of very large domain size for the computation. Xiao & Song (2019) studied the characteristics of these oblique turbulent bands in a channel flow domain of size upto $L_x \times L_z = 320h \times 320h$ using DNS and employing similar boundary conditions as used by Tao et al. (2018). They studied in detail the kinematics and dynamics of these localized turbulent bands for $Re_h = 750$ and provided a possible self-sustaining mechanism.

Table 1 summarizes some of the major experimental works conducted in the field of laminar-turbulent transition in channel flows. The result obtained in the current study is also shown for comparison. It can be seen that channels of different aspect ratios (AR), varying from 8 (Kao & Park, 1970) to 277 (Alavyoon et al., 1986), have been used in these previous experiments. In channels, the stability of the flow depends on the aspect ratio, the length, and the mode and amplitude of perturbation. Tatsumi & Yoshimura (1990) showed that the side-walls have a stabilizing effect on channel flow during transition, therefore increasing the aspect ratio reduces the critical Reynolds number by making the flow unstable at lower Reynolds number. In the physical experiments which must have finite size perturbations, the mode of disturbance also plays an important role in determining the critical Reynolds number. For example, Sano & Tamai (2016) used a channel flow facility of AR = 180, and by minimizing the perturbations, they could maintain laminar flow up to Reynolds number of $Re_h = 933$. However, when they used a grid at the inlet of the channel to provide a turbulent inlet condition they obtained a critical Reynolds number of about $Re_h = 553$. Nishioka et al. (1975) investigated transition in channel flow of AR = 27.4 by minimizing the background turbulence to a level of 0.05%. They employed hot-wire anemometry to investigate the linear and nonlinear instability, and breakdown to transition in channel flow. They could maintain laminar flow until $Re_h = 5333$ which is above the critical Reynolds number for linear stability ($Re_h = 3850$) as calculated by Orszag (1971). In addition to the very low background level, this difference was also attributed to the finite aspect ratio of the channel where the side-walls are known to have a stabilizing effect on the flow. Takeishi et al. (2015) studied the effect of aspect ratio on transition in rectangular duct flows. They showed

Table 1: Summary of major experimental works conducted in the field of laminar-turbulent transition in channel flows. Re_τ in the last column is calculated using the formula $Re_\tau = \sqrt{3Re_h}$, which is valid for laminar flows.

Authors	**Aspect Ratio**	**Transition mechanism**	**Transition characterisation technique**	**Critical** Re_h	**Critical** Re_τ
Patel & Head (1969)	48	Natural	Pressure drop and velocity	650	44
Kao & Park (1970)	8	Natural/artifical excitation	Velocity	731	47
Carlson et al. (1982)	133	Artificial excitation	Flow visualization	667	45
Alavyoon et al. (1986)	166; 277	Artificial excitation	Flow visualization	733	47
Tsukahara et al. (2014)	40	Turbulence grid	Flow visualization	650	44
Sano & Tamai (2016)	180	Artificial excitation	Flow visualization	553	41
Current study	11.9	Natural	Wall shear stress	609	43

that the lowest Reynolds number of sustained localized turbulence decreases monotonically with increasing aspect ratio of AR = 1 (square duct) until it reaches an almost minimum value for AR = 5. The localized structure was found to look similar to "puffs" (akin to those found in pipe flow) and "spots" for AR = 1-3 and AR = 5-9, respectively.

As discussed above, transition to turbulence in channel flows can start due to finite amplitude perturbations which give rise to turbulent spots and these localized structures show transient growth over the streamwise length of the channel (Lemoult et al., 2013; Sano & Tamai, 2016). Therefore, the meaning of "fully-developed" flow (which is generally defined as flow invariance in the streamwise direction, see for example Durst et al., 2005), seems to be ambiguously defined during the onset of transition where, by definition, there is spatial intermittency. Investigation of development lengths in laminar and fully-turbulent channel flows have been studied by many researchers in the past. Durst et al. (2005) proposed a correlation for the calculation of development length in laminar channel flows using a numerical technique. Dean (1978) compiled data from the previous experiments in channel flows and found that the entrance length varies from $46h$ to $600h$. Lien et al. (2004) recommended the development length to be $300h$ using velocity profile measurements in turbulent channel flow. In channel flows, pressure drop-measurements are typically used to calculate the mean wall shear stress and friction factor assuming the flow to be streamwise invariant. Previous researchers have employed pressure-drop measurement to study the transition in channel flow (Davies & White, 1928; Patel & Head, 1969). However, to the best of our knowledge, the effect of development length on pressure-drop measurements in transitional channel flows has still not been reported.

Deciding on when the flow has left a "transitional" state and entered a "fully-turbulent" state in a channel flow has remained an open question. Patel & Head (1969) discuss the different definitions for fully-turbulent channel flow: the disappearance of intermittency, the emergence of $-1/6$ power law scaling for skin friction and Reynolds number, and log-law relationship with universal constants for the mean velocity profile. From their experiments on channel flows they obtained different values of Reynolds number for the first sight of disappearance of intermittency ($Re_h \sim 1800$), skin friction agreement with $-1/6$ power law (Re_h = 2500-3000) and log-law relation with universal constants ($Re_h \sim 3000$). Carlson et al. (1982), using flow visualization, observed fully-turbulent flow by Re_h = 2000. Seki & Matsubara (2012) defined the term "marginal" Reynolds number based on sustainment of turbulent flows and showed that for the channel flow the upper value of marginal Reynolds number (Re_h) is 1300. Kushwaha et al. (2017) used DNS in channel flow and observed that by $Re_h = 993$, the flow was significantly three-dimensional and consisted of fluctuations throughout the computational domain. Tsukahara et al. (2014) carried out flow visualization to study the "stripy" structures in a channel flow. For $Re_h = 1200$, the flow appeared to be similar to a high-Reynolds number turbulent flow i.e. no apparent large-scale structure typically associated with transitional channel flow. On decreasing the Reynolds number the laminar-turbulent bands or turbulent stripes started to appear below $Re_h = 1000$.

In the present study, the transition process in a channel flow is investigated at the wall using time-resolved wall shear stress measurements. Previous studies rarely, if ever, reported the characteristics of the flow at the wall of the channel during transition. This is generally attributed to the practical challenges in conducting spatially and temporally well-resolved measurements of wall shear stress (Alfredsson et al., 1988). It has been found that there is a potential connection between the instantaneous wall shear stress and coherent motions of the flow above the wall in wall-bounded flows (Marusic et al., 2010; Orlu & Schlatter, 2011). Therefore, it has become important to have a better understanding of the instantaneous wall shear stress in order to understand the complex nature of transition to turbulence in shear flows. For channel flows, wall shear stress measurements are rather limited, especially, near transition and the lowest Reynolds number at which the higher order statistics of wall shear stress is studied is by Keirsbulck et al. (2012) for Re_h = 1055. Gubian et al. (2019) carried out wall shear stress measurements in a channel flow for $250 \leq Re_\tau \leq 930$ and observed that the statistical moments, probability density functions and spectra of wall shear stress reach an almost asymptotic value after $Re_\tau \sim 600$. Wall shear stress measurements were carried out in a channel flow using hot-film sensors by Whalley et al. (2019) at $Re_h(Re_\tau)$ = 1000(70), 1200(85) and 1500(100). They investigated the so-called low- and high-drag events in channel flow near transition using simultaneous measurements of velocity (using laser Doppler velocimetry, LDV or PIV) and

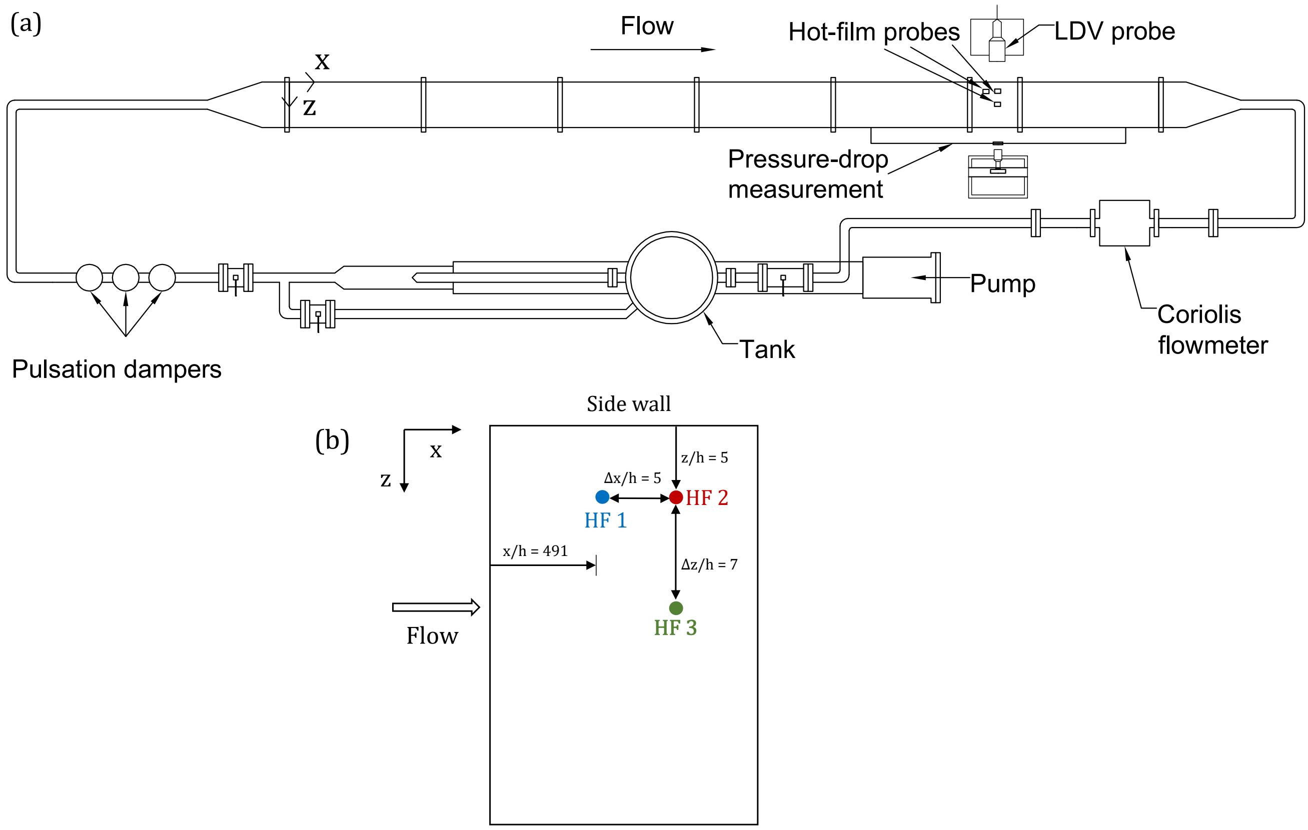

Figure 1: (a) Schematic of channel flow rig (not to scale). (b) Schematic of the hot-film arrangements in the test-section of our channel flow facility (not to scale).

the wall shear stress. The current study extends their analysis, using the same flow facility, by measuring the wall shear stress across a significantly wider Reynolds number range in the laminar-turbulent transition regime. Simultaneous measurements of wall shear stress for three spatial locations, as opposed to a single hot-film measurement carried out by Whalley et al. (2019), are also carried out in the present study.

Therefore, in the present study, an experimental investigation of instantaneous wall shear stress characteristics for transitional channel flow using hot-film anemometry is conducted. Using single-point statistics of wall shear stress fluctuations, an attempt is made to characterize the "start" and "end" of transition in our channel flow facility. Using spatial correlations of the wall shear stress at different locations, a study into the localized transitional structures is also carried out.

2. Experimental set-up

A closed-loop channel flow facility, at the University of Liverpool, is used in the present study which has a very similar arrangement as used by Whalley et al. (2017, 2019). A schematic of the channel flow facility is shown in figure 1(a). A rectangular duct with 6 stainless steel modules of 1.2 m length each and a test section of 0.25 m length are used, providing a total length of 7.45 m. The modules are connected using angle irons and threaded bars. Four threaded bars are used (two on the top side of the channel and two on the bottom) to attach each pair of modules. An O-ring is used to ensure that there is no leakage of the fluid and a hydraulically smooth transition between the modules. The modules are then aligned carefully using a laser targeting device. The full-height ($2h$) and full-width (w) of the channel are 0.025 m and 0.298 m, giving an aspect ratio ($w/2h$) of 11.92. The test-section has transparent windows on the top and side walls which provide optical access for the LDV measurements.

A glycerine-water mixture, of concentration approximately 52% (by weight) glycerine, is used as the working fluid. The fluid is stored in a stainless steel header tank and is pumped using a mono type E101 progressive cavity pump. The fluid passes through three pulsation dampers, to reduce the level of disturbances, before entering the channel. There is also a mixing loop connected to the pump which provides an opportunity to obtain lower flow rates. A Coriolis mass flow meter is installed in the return loop which is used to measure the mass flow rate. A platinum resistance thermometer (PRT) is connected to the last module of the channel to monitor the temperature of the working fluid during the experiment. Density and viscosity of the working fluid are measured using an Anton Paar DMA 35N density meter and an Anton Paar MCR 302 rheometer, respectively. Indicative values for the density and viscosity of the working fluid are 1130 kg/m^3 and 6.7 mPa.s, respectively at temperature, T = 19 ^{o}C. Pressure-drop measurement is carried out using a Druck LPX-9381 differential pressure transducer having a working range of 5 kPa and an accuracy of ±5 Pa. To study development length effects, pressure-drop measurements are compared for four different streamwise locations of the upstream pressure tap (x/h = 406, 312, 216, 120) and the downstream pressure tap remains at a fixed location, downstream of the measurement section, at x/h = 572. Pressure-drop data is acquired for 10 minutes for each Reynolds number. Further discussion regarding development length effects on pressure-drop measurements are provided in section 3. The pressure transducer is regularly calibrated against an MKS Baratron differential pressure-transducer.

Velocity measurements are carried out using LDV employing a Dantec FiberFlow laser system which uses a 300 mW argon-ion continuous wave laser. It has a 60X40 laser light transmitter, a 60X10 probe, a 55X12 beam expander and a 55X35 photomultiplier tube. The LDV is operated in forward-scatter mode. Measurement of instantaneous wall shear stress is carried out using hot-film anemometry (HFA) with 55R48 glue-on probes, manufactured by Dantec Dynamics. These probes are operated in constant temperature (CT) mode and are powered using a Dantec Streamline Pro velocimetry system. To avoid issues related to the sensitivity the hot-film sensors are glued on an "insert" made of delrin (a type of thermoplastic with low conductivity) and then the insert is connected to the bottom wall of the channel via precision-machined ports. The streamwise and spanwise lengths of the sensing element of these probes are 0.1 mm and 0.9 mm. In viscous units, these dimensions correspond to a streamwise length of Δx^+ = 0.67 and a spanwise length of Δz^+ = 6.06 for Re_τ = 84.2, which is the largest Reynolds number studied in the present work. In the present anemometer, the bridge ratio and the overheat ratio are set to be at 10 and 1.1, respectively. The typical frequency response of the anemometer is found to be around 20-30 kHz. The hot-film and LDV data are sampled simultaneously using a Dantec Burst Spectrum Analyzer at a typical sampling frequency of around 300 Hz. In viscous time units, this frequency corresponds to $\Delta t^+ \approx 1$ for Re_τ = 84.2 and this sampling frequency is therefore considered to be sufficient to capture the smallest scales in the flow (Hutchins et al., 2009). The mean voltage output from the anemometer is calibrated against the mean pressure drop using the pressure transducer. The pressure-drop measurements are carried out between two pressure taps located 408h and 572h away from the inlet of the channel. The calibration points are fit with a third order polynomial. An example of a calibration plot is shown in figure 2. Constant temperature HFA is very sensitive to ambient temperature as it assumes that the temperature of the working fluid is constant during the experiment (isothermal assumption). Therefore, a heat exchanger is used to control the temperature of the fluid to a precision of ± 0.01°C throughout the experiment, to avoid any thermal drift in hot-film voltages. In case of non-thermal drifts observed in any of the hot-films during a long-run measurement, the technique discussed in Agrawal et al. (2019) is utilized for the correction of the drifted signal.

Identification of large-scale turbulent structures in transitional channel flow is conducted using simultaneous measurement of local instantaneous wall shear stress using three different hot-film probes, which are named as HF1, HF2 and HF3.

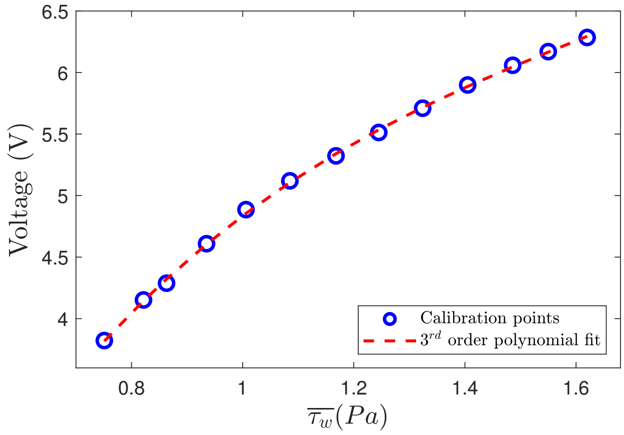

Figure 2: Calibration plot of mean hot-film voltage against mean wall-shear stress. The calibration curve is fit with a third order polynomial. The ambient fluid temperature is maintained at T = 19.10°C with a precision of ±0.01°C.

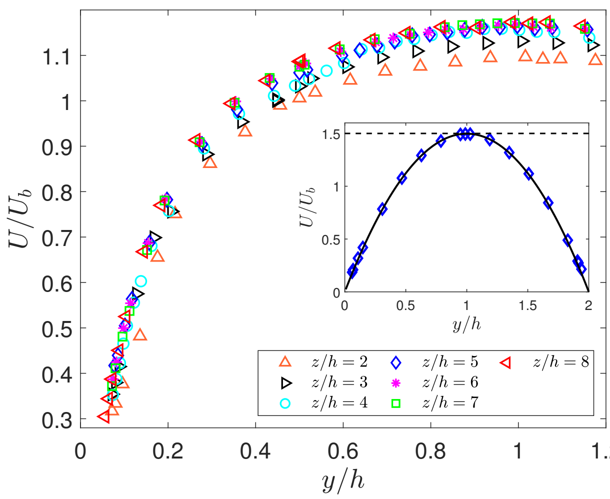

Figure 3: Normalized streamwise velocity profiles for Re_τ = 78 for spanwise locations of two channel half-heights to eight channel half-heights from the side-wall. Inset shows the velocity profiles obtained using experiment (indicated by blue diamonds) for Re_τ = 39. Solid black line and dashed black line indicate laminar theoretical profile and constant value of 1.5, respectively.

The arrangement of the three hot-films are shown in figure 1(b). HF1 and HF2 are located at the same spanwise location of z/h = 5 but different streamwise locations of x/h = 491 and 496, respectively. Here, z = 0 and x = 0 indicate the side-wall and inlet of the channel, respectively. HF3 is located at a spanwise location of z/h = 12 and streamwise location of x/h = 496. To check the effect of side walls, velocity profiles for Re_τ = 78 (Re_h = 1116) are measured for spanwise locations of z/h of 2 to 8. Each wall normal location is sampled for around 300 s at an average data rate of about 100 Hz. From figure 3 it can be seen that the velocity profiles approximately collapse after a spanwise distance of 4h. The inset plot of figure 3 shows that there is a good agreement between the velocity profile obtained for Re_τ = 39 (Re_h = 498) at z/h = 5 with the laminar theoretical profile. A DNS study by Vinuesa et al. (2015) shows the effect of side walls in channel flows by calculating the kinetic energy of secondary flows for Re_τ = 180. This kinetic energy was shown to approximately decay to zero after $z/h = 4$. Therefore, a spanwise location of more than $5h$ from the side wall can be considered to follow a 2-D channel flow approximation. Instantaneous wall shear stress measurements are conducted for Re_τ (Re_h) of 39.8 (510), 40.6 (541), 42.9 (609), 44.5 (642), 45.4 (673), 46.8 (706), 48.7 (738), 51.5 (763), 53.9 (807), 61.5 (887), 67.2 (969), 73.4 (1043), 79.3 (1125) and 84.2 (1213). Simultaneous wall shear stress data are acquired using the three hot-films for time durations of more than 100,000 convective time units ($tU_b/h > 100,000$) for every Reynolds number, where t indicates measurement time in seconds. This gives us the opportunity to calculate well-converged higher order statistics of wall shear stress during transition.

Uncertainty quantification for the pressure-drop measurements is carried out using the method provided by Kline & McClintock (1953). The Druck LPX-9381 pressure transducer has an accuracy of ±5 Pa, as quoted by the manufacturer. The typical value of pressure drop is 163 Pa corresponding to $Re_\tau = 51.5$. The present channel-flow facility is carefully machined to provide negligible relative uncertainties (≈ 0.15%) in the channel dimensions (w and h) and the length between the pressure tapings, l. Therefore, the relative uncertainty in the mean wall shear stress is $\Delta\tau_w/\overline{\tau_w} = 2 - 5\%$. The density ($\rho$) of the working fluid is measured using an Anton Paar DMA 35N density meter which has a quoted accuracy of ± 1 kg/m^3. This gives the relative uncertainty in the density of the working fluid as $\Delta\rho/\rho = 0.09\%$. The relative uncertainty in the viscosity (μ) measurement of the working fluid using Anton Paar MCR 302 rheometer is $\Delta\mu/\mu = 2\%$. The relative uncertainty in the friction velocity ($u_\tau = \sqrt{\tau_w/\rho}$) is $\Delta u_\tau/u_\tau$ = 1-2%. This gives an uncertainty in friction Reynolds number ($Re_\tau = u_\tau h/\nu$) measurement of $\Delta Re_\tau/Re_\tau$ = 3-4 %. Friction factor ($f = \tau_w/0.5\rho U_b^2$) has a relative uncertainty of $\Delta f/f = 2 - 5\%$.

3. Flow development length during transition for pressure-drop measurements

Accurate pressure-drop measurements are essential as the hot-film voltages are calibrated against the pressure-drop data to obtain instantaneous wall shear stress signals. The hot-film and the pressure-drop measurements should be conducted in the so-called "fully-developed" region of the flow. We investigate the development length requirements for the pressure-drop measurements in our channel flow facility for Reynolds number (Re_h) between 515 and 1460. Pressure-drop measurements are conducted for four different upstream pressure taps L_{us}/h = 120, 216, 312 and 408 while the downstream pressure tap is kept at a constant location of $L_{ds}/h = 572$, where L_{us} and L_{ds} represent the distance of the upstream and downstream pressure taps from the channel inlet, respectively. Fanning friction factor ($f = \tau_w/0.5\rho U_b^2$) is calculated from the mean wall shear stress ($\tau_w = \Delta P w(2h)/(2l(w + 2h))$, where ΔP is the mean pressure drop over length (l) and bulk velocity (U_b) for each Reynolds number. The laminar theoretical value for the fanning friction factor, i.e. $f = 6/Re_h$ can be obtained using the assumption that the flow is parabolic for the laminar flow. Figure 4(a) shows the variation of f with Re_h for various locations of upstream pressure taps and figure 4(b) shows the relative error of f compared to the laminar theoretical values ($(f - 6/Re_h)/(6/Re_h)$) with Re_h for various locations of upstream pressure taps. The empirical correlation obtained by Dean (1978), based on an extensive literature review, for turbulent channel flows is shown for comparison. Pope (2000) obtained an approximate relation between the length scales of mean flow and viscous flow for turbulent channel flow, given by $Re_\tau \approx (2Re_h)^{0.88}$. This relation is converted to obtain a relation between f and Re_h and is shown in figure 4. There are two effects which are both playing a role in the variation of the Fanning skin-friction coefficient (f) with L_{us}/h for the same bulk Reynolds number (Re_h) as shown in figures 4(a) and 4(b). First is the flow-development region which is generally associated with the streamwise length required for the flow to become fully-developed (Durst et al., 2005). It can be seen that for a streamwise distance of the upstream pressure tapping of $L_{us}/h = 120$, f is significantly higher than for $L_{us}/h \geq 216$ for $Re_h \leq 600$. As will be discussed in the next section, the flow remains laminar up to $Re_h \approx 610$ in the present channel flow facility. This suggests that for the Reynolds numbers when the flow is laminar, for the streamwise distance of $L_{us} = 120h$ the flow is still developing and after $L_{us} = 216h$ the flow can be considered to be fully-developed.

Second is the effect of spatial inhomogeneity of the flow for the transitional Reynolds numbers (Carlson et al., 1982; Sano & Tamai, 2016) which has a significant effect for $600 \leq Re_h \leq 1000$ on the friction factor. From figure 4(a,b) it can be seen that after $Re_h \approx 600$, f becomes more sensitive to L_{us}/h as f keeps decreasing with increasing L_{us} and for $Re_h \approx 770$ the difference is most significant. This behaviour can be attributed to the presence of large-scale intermittencies generally associated with spatially inhomogeneous structures near the onset of transition. For example, Carlson et al. (1982) and Sano & Tamai (2016) showed that near the critical Reynolds number artificially-generated finite amplitude perturbations grew or decayed (based on the Reynolds number) as they moved downstream. Therefore, the turbulent structures which are present at the inlet near the critical Reynolds number may decay as they flow downstream and thus reduce the value of f for higher L_{us}, as f is lower for laminar flow compared to turbulent flow for the same Re_h. After $Re_h \approx 770$, the effect of these large-scale intermittencies during transition starts to decrease gradually and after $Re_h \approx 1000$, the friction factor values start to collapse for $L_{us}/h \geq 216$. Thus, it can be said that it is difficult to define a "development length" (i.e. when the flow becomes independent of x) during transition which by its very nature is spatially inhomogeneous (i.e. the flow necessarily varies in x). Based on the above discussion, the farthest streamwise location of $L_{us}/h = 408$ is chosen for the pressure-drop measurements in the present experiment. It is also observed that the friction factor values do not seem to collapse for the $Re_h \approx 1400$ to the results given by Dean (1978) and Pope (2000). This is believed to be the consequence of low Reynolds number effects as Dean (1978) also observed a large scatter in the data for similar Reynolds numbers and after $Re_h = 3000$ the empirical correlation worked well in being an accurate description of the skin-friction for channel

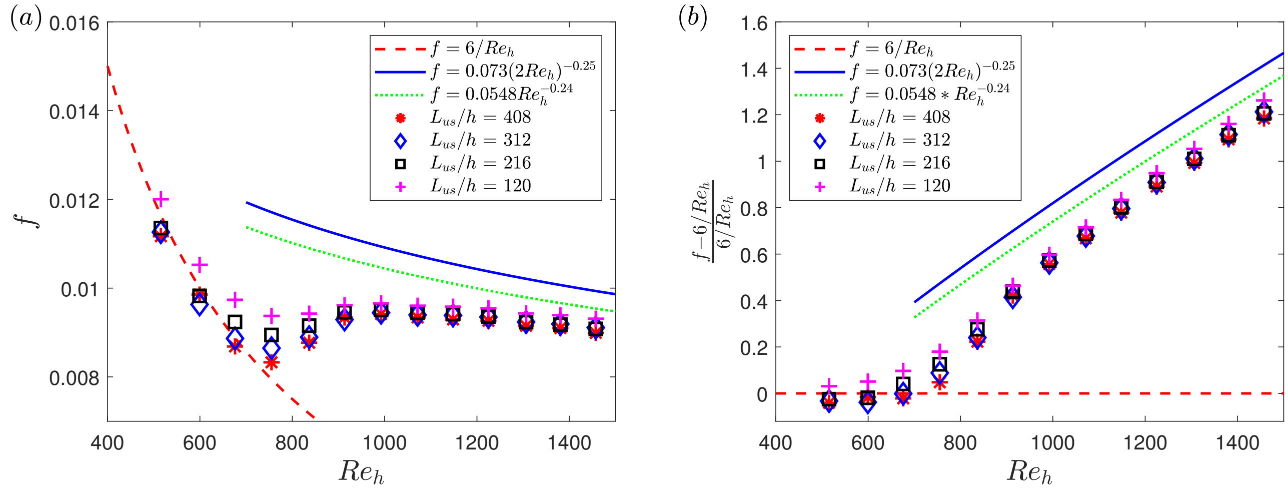

Figure 4: (a) Fanning friction factors against Reynolds number for different locations of upstream pressure tap. Red dashed line represents theoretical laminar friction factor. Green dotted line and blue solid line show the correlations obtained from Pope (2000) and Dean (1978), respectively. (b) Variation of the fractional error in the friction factor from the theoretical laminar friction factor with the Reynolds number for different locations of upstream pressure tap. Symbols and lines represent same quantities as in (a).

flows.

4. Time history and single-point statistics of wall shear stress in transitional channel flow

In this section, results obtained from a single hot-film measurement, HF2, located at $z/h = 5$ and $x/h = 496$, are discussed. As a first step of investigating the wall shear stress behaviour for the transitional Reynolds numbers, their segments of time histories for various Reynolds numbers are studied. A careful study of the time history will also make analysis of statistical properties of wall shear stress fluctuations easier to interpret. Figure 5 shows segments of instantaneous normalized wall shear stress for various Reynolds numbers where τ'_w and $\overline{\tau_w}$ represent the instantaneous wall shear stress fluctuations and time-averaged wall shear stress, respectively. This plot also shows the corresponding values of normalized intensity of the wall shear stress fluctuations, indicated by the root mean square of the wall shear stress fluctuations, $\sigma(\tau'_w)$. It can be observed that there are no significant fluctuations in wall shear stress for $Re_\tau = 40.6$ and 42.9, which is also shown by the $\sigma(\tau'_w)/\overline{\tau_w}$ values lower than 0.01 for these two Reynolds numbers. So it can be said that the flow is in the laminar state at these values of Reynolds numbers. For $Re_\tau = 44.5$ the appearance of some small amplitude fluctuations start and at $Re_\tau = 45.4$ and 46.8, large amplitude fluctuations emerge in an otherwise laminar background. It is postulated that these large amplitude fluctuations represent the localized turbulent structures which sustain themselves up to at least a streamwise distance of $x/h = 496$ as they flow downstream from the inlet. Patel & Head (1969) observed a similar phenomena of apparently random appearance of large amplitude fluctuations in their hot-wire data at the onset of transition in channel flows and they called these large amplitude fluctuations "turbulent bursts". The frequency of these localized structures is observed to increase with increasing Reynolds numbers of $Re_\tau = 48.7$, 51.5 and 53.9, as shown in figure 5(f,g,h). For these Reynolds numbers the flow can be seen to be highly intermittent, frequently switching between laminar and localized turbulent states. By $Re_\tau = 67.2$ laminar flow is almost entirely absent and the flow can be seen to consist mostly of turbulent events. This indicates the disappearance of laminar-turbulent intermittency at higher Reynolds numbers.

To further investigate the characteristics of wall shear stress fluctuations, higher order statistics and probability density functions (PDFs) of wall shear stress are calculated. The second order statistics, as also discussed earlier, is given by the RMS of wall shear stress fluctuations. As can be seen from figure 6, $\sigma(\tau'_w)/\overline{\tau_w}$ values are observed to increase monotonically from $Re_\tau = 44.5$ to $Re_\tau = 84.2$. But a significant decrease in the rate of change is observed at $Re_\tau \approx 53$. This significant difference in the rate of change of the RMS values can be explained based on the time histories of wall shear stress as shown in figure 5. It can be observed that until $Re_\tau \approx 53.9$, the signals are highly intermittent and after this Reynolds number the signal starts to become uniformly turbulent and therefore the rate of change of RMS of wall shear stress fluctuations also starts to decrease. Third and fourth order moments of wall shear stress fluctuations, i.e. the skewness $S(\tau'_w)$ and flatness (or kurtosis) $F(\tau'_w)$, respectively, are given by $S(\tau'_w) = \overline{\tau'^3_w}/\sigma(\tau'_w)^3$ and $F(\tau'_w) = \overline{\tau'^4_w}/\sigma(\tau'_w)^4$. Figure 7 shows the skewness and flatness of wall shear stress fluctuations for various Reynolds numbers. From figure 7(a) and (b) it can be seen that for $Re_\tau \leq 42.9$, $S(\tau'_w) \simeq 0$ and $F(\tau'_w) \simeq 3$, thus indicating the presence of laminar flow, as for a Gaussian signal the skewness and flatness values are 0 and 3, respectively (i.e. our background noise is likely to be white-noise). There is a sharp increase in the skewness and flatness of wall shear stress for $Re_\tau \geq 44.5$ which can be correlated with figure 5(c, d). As already discussed before, it can be seen that there are few fluctuations at these Reynolds numbers which leads to very

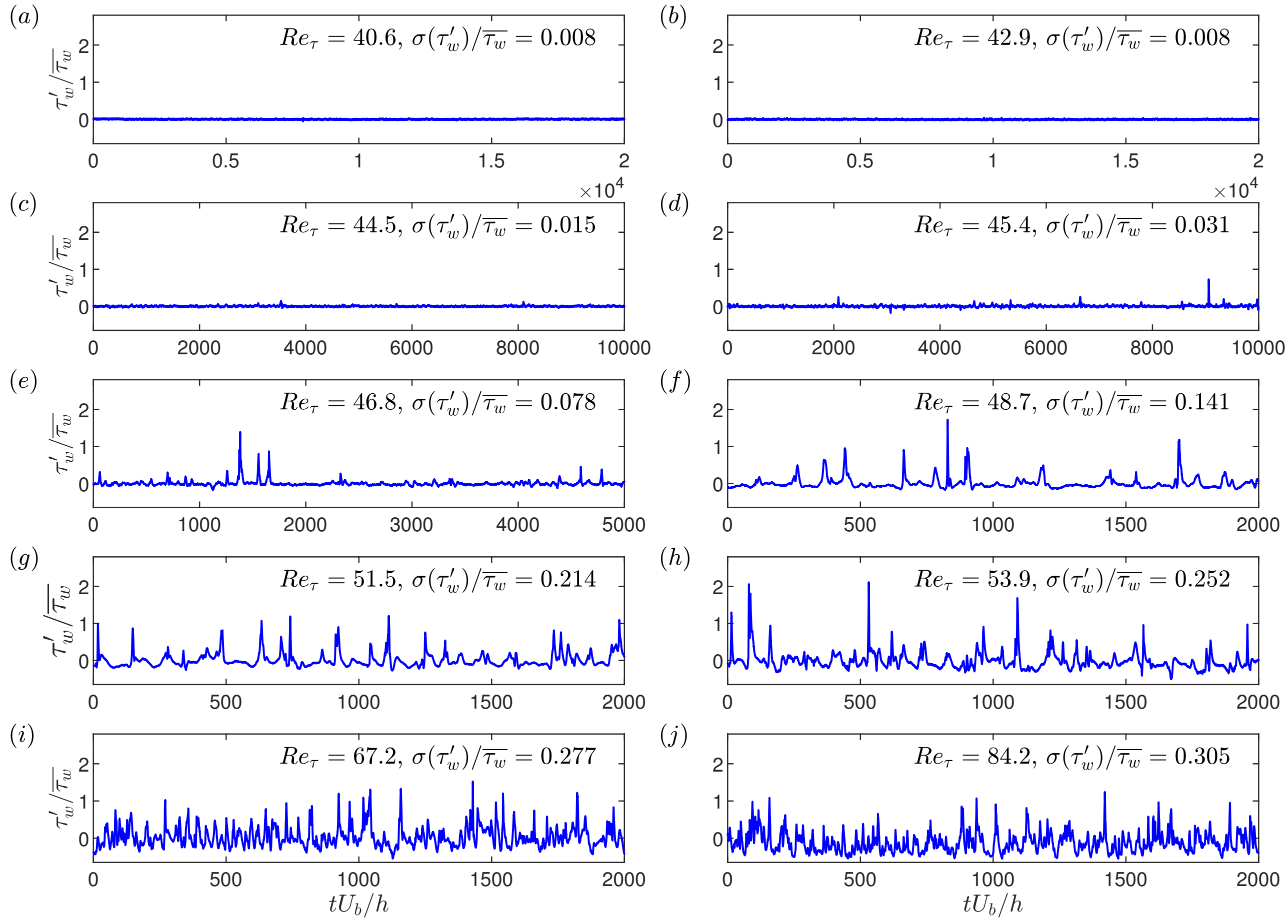

Figure 5: Segments of instantaneous normalized wall shear stress fluctuations measured using HF2 located at $z/h = 5$ and $x/h = 496$ for various Reynolds numbers. The plots also show the corresponding values of normalized RMS of wall shear stress fluctuations.

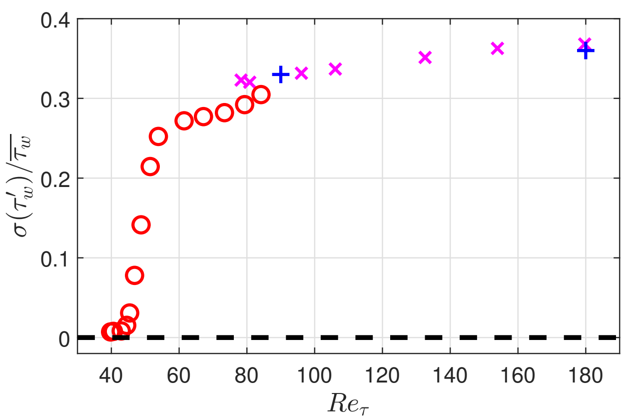

Figure 6: Normalized root mean square of the wall shear stress fluctuations for various Reynolds numbers where red circles, purple crosses and blue pluses indicate the data obtained by the present experiment, Keirsbulck et al. (2012) and Hu et al. (2006), respectively.

high values of skewness and flatness of the signals as shown in figure 7. For Re_τ close to 48 the skewness and flatness peak to a very high magnitude. This high magnitude indicates a very high level of laminar-turbulent intermittency in the flow. And for increasing Reynolds numbers the third and fourth order moments start to decrease which indicates the increasing dominance of turbulent events in the flow and thus decreasing intermittency (as can also be seen from figure 5). Jovanović et al. (1993) carried out a least-square fit of the skewness and flatness of the streamwise velocity data obtained in previous studies for pipe, channel and boundary layer flows and obtained the relation $F \simeq 2.65 + 1.62S^2$ (note F does not go to a value of three as S tends to zero which is explained as a consequence of the least-square fit). A good agreement is observed with the least square fit (obtained from the streamwise velocity data) and the present experimental data for wall shear stress, as shown in figure 7(c). One interesting point to note is that the least-square conducted by Jovanović et al. (1993) contained maximum values of S^2 and F data as 4 and 8 respectively but the present result shows that this relation still provides a good approximation for very high magnitudes of skewness and flatness i.e. $S^2 \sim 50$ and $F \sim 10^2$. Figure 6 and 7 also show the data obtained by Keirsbulck et al. (2012) and Hu et al. (2006) who employed an electrochemical technique and

DNS, respectively to investigate wall shear stress fluctuations in channel flow. For $Re_\tau > 73.4$, the trend of the moments obtained using the present experiment seem to approach the values given by Hu et al. (2006) and Keirsbulck et al. (2012) with a slight discrepancy especially in the second and fourth moments. This discrepancy is speculated to arise because of the limited frequency response, and spatial and temporal resolutions of the hot-film probes (Alfredsson et al., 1988). Figure 8(a) and 8(b) show the probability density functions (PDFs) of normalized wall shear stress ($\tau_w/\overline{\tau_w}$) and normalized wall shear stress fluctuations ($\tau'_w/\sigma(\tau'_w)$), respectively. Figure 8(a) shows that for $Re_\tau \lesssim 42.9$, the PDFs of normalized wall shear stress values collapse onto each other with the maximum value of the PDF lying on about $\tau_w/\overline{\tau_w} = 1$, thus indicating the flow to be in a laminar state. This result is consistent with the time history and higher-order moments results discussed earlier. The PDF for $Re_\tau = 44.5$ deviates from the laminar PDF, which shows the presence of finite amplitude fluctuations in the flow. The PDF for $Re_\tau \geq 44.5$ has a longer tail for the values above the mean for all the given Reynolds numbers thus giving rise to positive skewness. Figure 8(b) shows that there is a slight Reynolds number dependency between the PDFs for $Re_\tau = 73.4$ and $Re_\tau = 79.3$, which can also be seen from their skewness and flatness values in figure 7(a,b). But for $Re_\tau \geq$ 79.3 there is no significant Reynolds number dependency on the PDFs of normalized wall shear stress fluctuations. This is consistent with results by Kushwaha et al. (2017) and Tsukahara et al. (2014) where it is shown that the large scale "stripy" structures in the flow seem to disappear as the Reynolds number increases beyond $Re_\tau \sim 70$ and gradually the flow becomes uniformly turbulent. The present result is also compared with the DNS result by Hu et al. (2006). There seems to be a good agreement between the PDF obtained by Hu et al. (2006) for $Re_\tau = 90$ and present experiment for $Re_\tau = 84.2$, but, as discussed previously the slight differences might be caused by the limited frequency response and spatial and temporal resolution issues of our hot-film probes. Therefore, from the higher order statistics and PDF of wall shear stress it can be said that any significant Reynolds number dependency of the flow fluctuations during transition have started to disappear by friction Reynolds number value somewhere between 73.4 and 79.3.

5. Wall footprint of large-scale turbulent structures in transitional channel flow

Simultaneous measurements using three different hot-films are conducted to investigate the characteristics of the large-scale turbulent structures in our channel-flow facility for transitional Reynolds numbers. The locations of the three hot-films (HF1, HF2 and HF3) were shown in figure 1(b). Figure 9 shows the segments of normalized wall shear stress fluctuations for $Re_\tau = 48.7$, 51.5 and 61.5, which are obtained simultaneously using the three hot-films. It can be seen that for $Re_\tau = 48.7$ some of the large amplitude fluctuations appear to occur almost simultaneously at all the three hot-film locations with some time lags. This suggests the presence of large-scale structures which are at least 7 channel half-heights wide. This seems to be consistent with the previous studies where the presence of large-scale turbulent structures called turbulent spots have been observed near the onset of transition (Carlson et al., 1982; Aida et al., 2010; Sano & Tamai, 2016). Although the AR of our channel is ≈ 12, it is believed that this aspect ratio is enough to have sustained localized structures during transition. Takeishi et al. (2015) showed the presence of turbulent spots for $AR \geq 5$ similar to those in channel flows of very large aspect ratio, for example Carlson et al. (1982) and Tsukahara et al. (2014). In figure 9(a), some of the large amplitude fluctuations can be seen to not occur in all three hot-film signals. This is not unexpected because these structures are found to be localized not only in the streamwise direction, but also in the spanwise direction (Sano & Tamai, 2016; Patel & Head, 1969). Therefore, it is possible that for some instances one hot-film (e.g. HF2) cannot detect the presence of a turbulent spot passing by the HF3, which is located at another spanwise location or vice versa. From figure 9 (b, c) it can be seen that there is a decreasing number of such high amplitude fluctuations occurring simultaneously with increasing Reynolds numbers. Cross-correlations of the wall shear stresses for all combinations of spatial location pairs are conducted. To calculate cross-correlations, instantaneous wall shear stress is converted to the corresponding friction velocity using the relation $U_\tau = \sqrt{\tau_w/\rho}$. The fluctuating friction velocities are then calculated by subtracting the time-averaged friction velocity from the instantaneous values, $u_\tau = U_\tau - \overline{U_\tau}$. The cross-correlation is then calculated using equation 1.

$$R_{u_{\tau_i}u_{\tau_j}} = \frac{\overline{u_{\tau_i}(t)u_{\tau_j}(t+\Delta t)}}{\overline{u_{\tau_i}(t)u_{\tau_j}(t)}} \tag{1}$$

where u_{τ_i} and u_{τ_j} represent friction velocities calculated using wall shear stress measurements from two of the three hot-films and Δt represents the time-lag. Here the subscript i and j can take values 1, 2 or 3 which represents the hot-films HF1, HF2 and HF3, respectively. Figure 10 shows the cross-correlations of friction velocities for the same spanwise location of $z/h = 5$, but two different streamwise locations of $x/h = 491$ and 496, which are obtained using HF1 and HF2. It can be seen that the magnitude of the peak of the correlations decreases with increasing Reynolds numbers, which can be explained based on the increasing fluctuations and thus lower correlations with increasing Reynolds numbers. It is also observed that there is a lag in the peak of correlations for all the Reynolds numbers. The streamwise separation between the probes has been used to estimate the convective (or propagation) velocity of the flow previously by Krogstad et al. (1998). They observed that the obtained value of convective velocity changes with changing probe separation distance because the convective velocity of the flow depends on the scale of motion. Therefore, the measurement can be biased towards motion of large scales if a larger probe distance is chosen as they dominate the correlation. In the present study the convective velocity calculated from the correlation is used to convert the time lag to a spatial separation using equation 2.

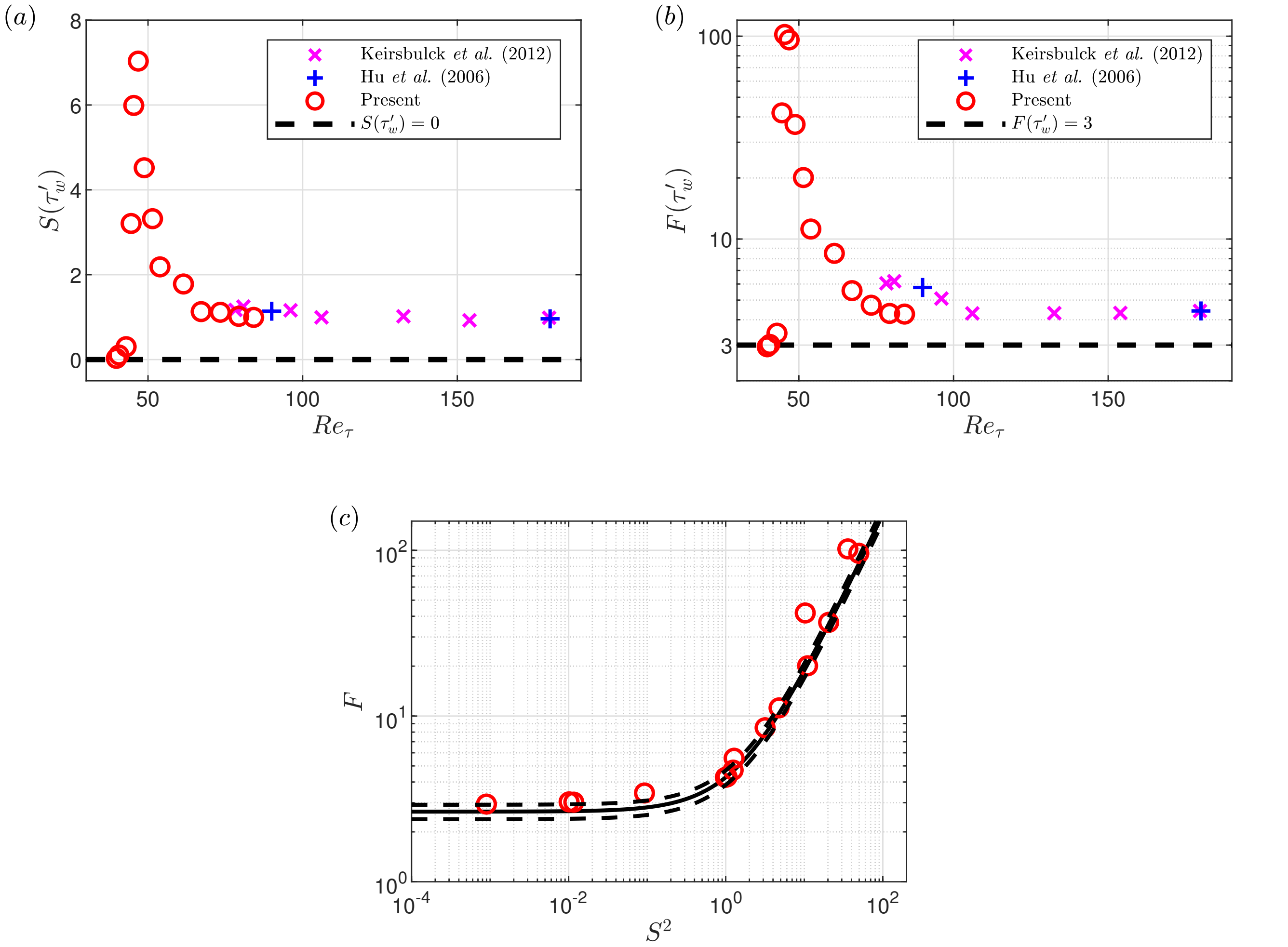

Figure 7: (a) Variation of skewness with Reynolds number; (b) Variation of flatness with Reynolds number; (c) Relation between flatness and skewness^2 where the solid line indicates the emperical relation obtained by Jovanović et al. (1993) for streamwise velocity data: $F \simeq 2.65 + 1.62S^2$, the dashed lines indicates $\pm10\%$ of $F \simeq 2.65 + 1.62S^2$ and red circles represent the moments of wall shear stress data obtained from the present experiment.

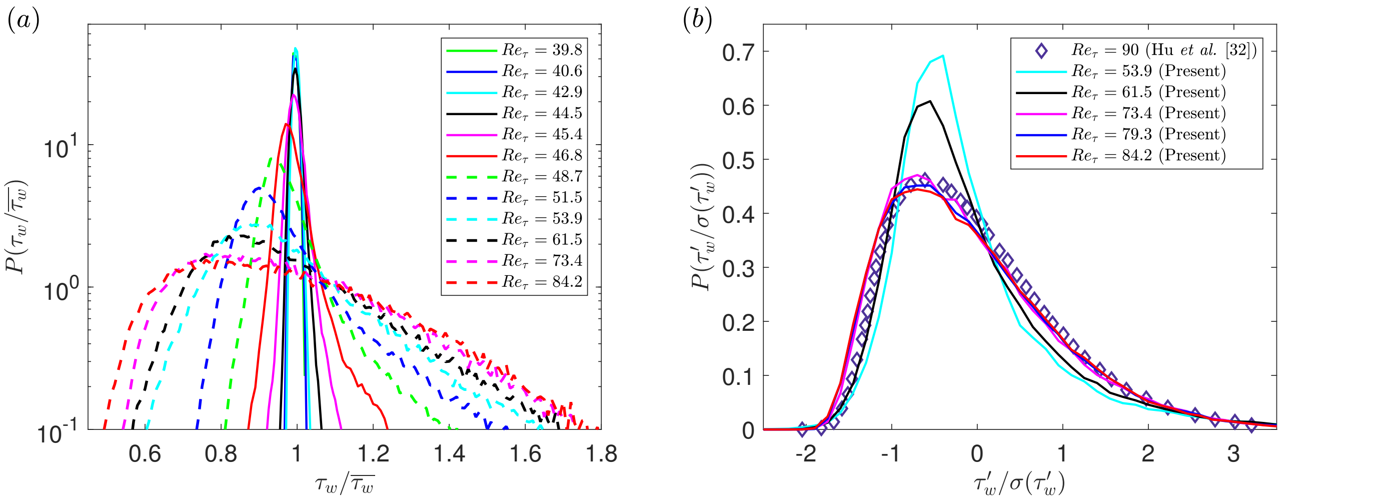

Figure 8: PDFs of normalized wall shear stress for varying Reynolds numbers. (b) PDFs of normalized wall shear stress fluctuations for varying Reynolds numbers.

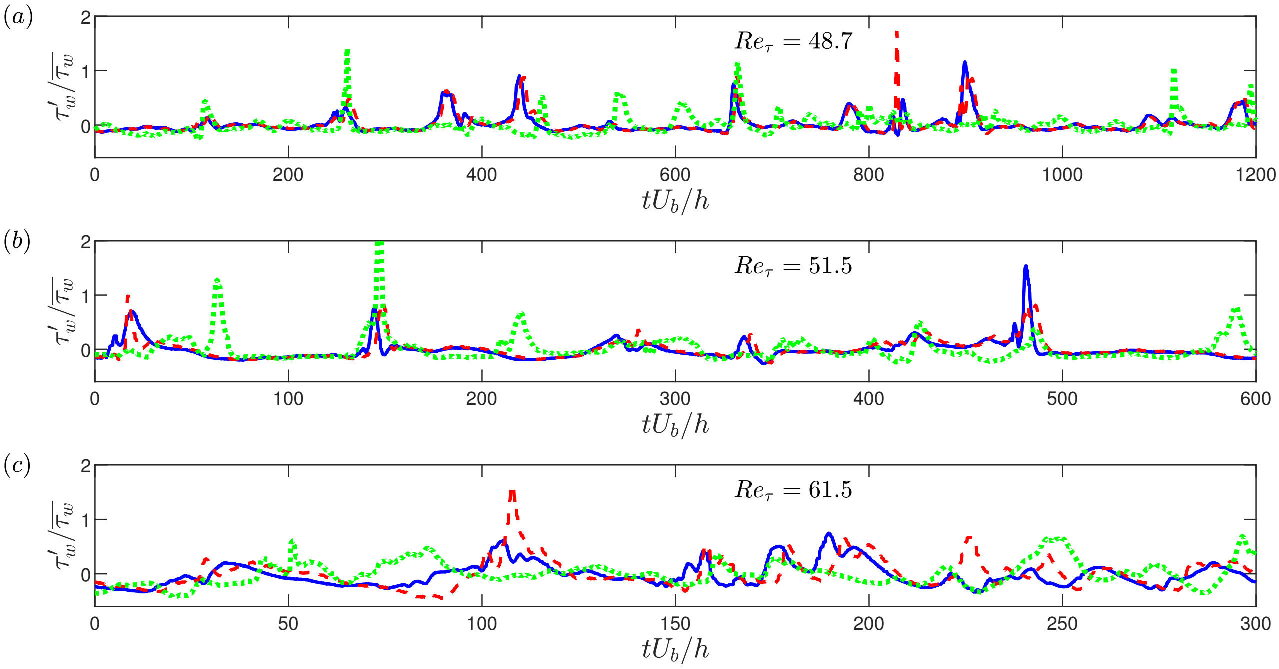

Figure 9: Segments of normalized wall shear stress fluctuations for (a) $Re_\tau = 48.7$, (b) $Re_\tau = 51.5$ and (c) $Re_\tau = 61.5$, where blue solid lines, red dashed lines and green dotted lines represent data obtained using HF1, HF2 and HF3, respectively.

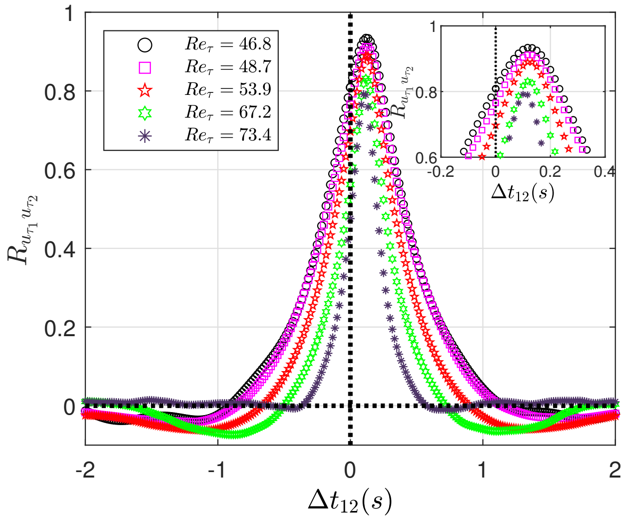

Figure 10: Cross-correlations of friction velocities calculated using the wall shear stress from the streamwise-aligned hot-films: HF1($x/h = 491; z/h = 5$) and HF2($x/h = 496; z/h = 5$).

$$U_c = 5h/\Delta t_{12,max} \tag{2}$$

where $\Delta t_{12,max}$ is the temporal separation for which the $R_{u_{\tau_1} u_{\tau_2}}$ is maximum. Figure 9 shows that there occurs almost simultaneous large amplitude fluctuations in the wall shear stress time history data obtained from hot-films HF2 and HF3 for $Re_\tau = 48.7$. These two hot-films are separated in the spanwise direction with a gap of $7h$ and are at the same streamwise distance of $496h$ from the inlet. Figure 11(a) shows the correlation of wall shear stress obtained at these two spatial locations. It can be seen that there is a significant correlation of the wall shear stresses for Re_τ between 46.8 and 53.9 which indicates the presence of large-scale turbulent structures in this range of Reynolds numbers which are at least $7h$ large. It can also be seen that there is a positive lag in the correlation coefficient which shows that the same structures do not occur directly above both of the hot-films at the same time, but there is some delay. Since correlation is an integral measure, the lag indicates the structures are, on average, inclined in the $x - z$ plane. For $Re_\tau \geq 61.5$ the correlation peak has a magnitude lower than 0.05, thus indicating no significant correlation. A similar correlation is also conducted for HF1 and HF3 and is shown in figure 11(b). This figure shows very similar behaviour as figure 11(a), which is expected because HF1 and HF2 lie at the same spanwise location but are separated by a streamwise distance of $5h$. Table 2 shows the laminar centerline velocity ($U_{cl,lam} = 1.5U_b$), and the convective velocity (U_c) obtained using equation 2 for Re_τ between 46.8 and 73.4. Table 2 also shows the time lags (in seconds) between each pair of hot-film locations for Re_τ between 46.8 and 53.9. Time lags $\Delta t_{23,max}$ and $\Delta t_{13,max}$ indicate the temporal separation for which the $R_{u_{\tau_2} u_{\tau_3}}$ and $R_{u_{\tau_1} u_{\tau_3}}$ are maximum, respectively. Note that $\Delta t_{13,max} = \Delta t_{12,max} + \Delta t_{23,max}$ should be true theoretically. A nice agreement with the theoretical prediction is observed between the time lags and the minor differences with the theoretical prediction can be attributed to the uncertainty associated with the calculation of correlations. The time lag $\Delta t_{12,max}$ is observed to be independent of the Reynolds number for Re_τ between 46.8 and 53.9. This is because of the small steps in the increment of Reynolds number thus leading to the change in the $\Delta t_{12,max}$ within the measurement uncertainty. An attempt is made to calculate the average structure angles of the structures present during the onset

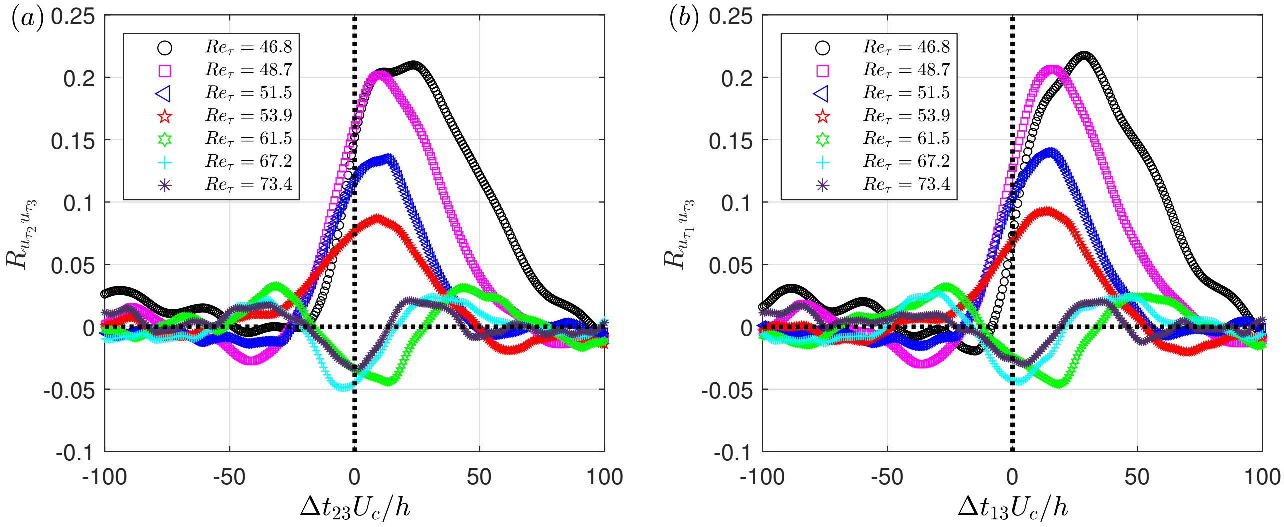

Figure 11: Cross-correlations of friction velocities calculated using wall shear stress data for (a) HF2 and HF3, (b) HF1 and HF3.

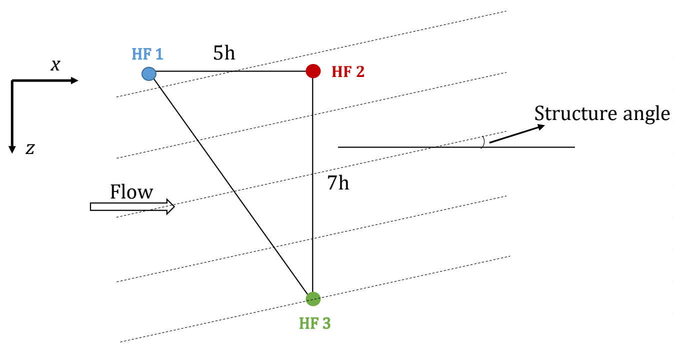

Figure 12: Schematic of the hot-film arrangements. The locations of the hot-films are shown in figure 1(b)

of transition. Figure 12 shows the hot-film arrangements with the assumed flow behaviour of the large-scale transitional structures passing through the three hot-films. Structure angles between the two-pairs of hot-films (HF2-HF3 and HF1-HF3) are calculated using equations 3 and 4, respectively.

$$\tan\theta_{23} = \frac{7\Delta t_{12,max}}{5\Delta t_{23,max}} \tag{3}$$

$$\tan\theta_{13} = \frac{7\Delta t_{12,max}}{5(\Delta t_{13,max} - \Delta t_{12,max})} \tag{4}$$

The structure angles obtained are shown in table 2. Here, the angles are calculated by carrying out a Gaussian fit near the peak of the correlations for all data. It should again be noted that theoretically $\theta_{23} = \theta_{13}$, i.e. the average structure angle obtained from the correlations between HF2-HF3 and HF1-HF3 should be the same. For $Re_\tau = 46.8$, the average structure angle obtained using both of the hot-films are about 17^o and the average structure angles for Re_τ between 48.7 and 53.9 are found to be between 32^o and 37^o. The discrepancy in angles obtained for $Re_\tau = 48.7$ and 51.9 by using two different correlations is an artefact of the discrepancy observed in the respective time lag calculations. This big change in angle is predicted to be a consequence of the significant change in the flow behaviour between these two Reynolds numbers. It can be seen from the single-point statistics of wall shear stress fluctuations, as shown in table 2, that the $\sigma(\tau_w')/\overline{\tau_w}$ value almost doubles and $S(\tau_w')$ peaks for $Re_\tau = 46.8$ and starts to decrease after this Reynolds number. Carlson et al. (1982), using flow visualization, observed oblique waves associated with the turbulent spots in channel flows. They obtained the angle of the leading-edge waves between 18^o and 25^o for lower Reynolds numbers and 37^o for higher Reynolds number. The angles obtained in the present study are in good agreement with the results obtained by Carlson et al. (1982). We predict that the average structure angles indicate the presence of oblique waves which are generally associated with turbulent spots (Carlson et al., 1982; Alavyoon et al., 1986; Li & Widnall, 1989; Aida et al., 2010). This also suggests that the turbulent spots observed in previous studies using flow visualization and velocity field measurements possess a significant wall footprint.

6. Conclusions

An experimental investigation of wall shear stress characteristics for transitional channel flow has been conducted using hot-film anemometry. The effect of development length shows that the entrance length has more significant impact near the onset of transition for the pressure-drop measurements. Single-point measurements of wall shear stress indicates that the time history is free of any significant perturbations in the flow for $Re_\tau \lesssim 42.9$, suggesting that the flow is in a laminar state. There is an appearance of high amplitude fluctuations beyond $Re_\tau = 42.9$, whose frequency seem to be increasing with increasing Reynolds numbers until the flow is seen to consist only of turbulent events by $Re_\tau = 67.2$. Skewness and flatness of wall shear stress fluctuations jumps at the onset of transition and reaches to a very high magnitude which is an indication of laminar-turbulent intermittency for these Reynolds

Table 2: Time lags (in seconds) of maximum peak locations between each pair of hot-films and average structure angles (in degrees) along the streamwise direction between each pair of hot-films. Second and third order moments of wall shear stress fluctuations, and the laminar centerline velocity ($U_{cl,lam}$) and the convective velocity (U_c) are also shown.

Re_τ	$U_{cl,lam}$ (m/s)	U_c (m/s)	$\sigma(\tau'_w)/\overline{\tau_w}$	$S(\tau'_w)$	$\Delta t_{12,max}$ (s)	$\Delta t_{23,max}$ (s)	$\Delta t_{13,max}$ (s)	θ_{23} (deg.)	θ_{13} (deg.)
46.8	0.51	0.51	0.078	7.03	0.12	0.57	0.69	17	17
48.7	0.53	0.52	0.141	4.52	0.12	0.26	0.39	33	32
51.5	0.56	0.50	0.214	3.32	0.12	0.26	0.36	34	37
53.9	0.59	0.51	0.252	2.18	0.12	0.23	0.34	36	36
61.5	0.65	0.52	0.272	1.78	-	-	-	-	-
67.2	0.71	0.55	0.277	1.13	-	-	-	-	-
73.4	0.76	0.59	0.282	1.11	-	-	-	-	-

numbers. After $Re_\tau \approx 48$, these two moments start to slowly decrease with increasing Reynolds number until there is no significant Reynolds number effects for $Re_\tau \simeq 73-79$. Simultaneous measurements of wall shear stress at three different locations indicate the presence of large-scale turbulent structures near the onset of transition. The average angles of these large-scale structures near the onset of transition are estimated using two-point correlations and the values obtained are about 17^o for $Re_\tau = 46.8$ and between 32^o and 37^o for $Re_\tau = 48.7$ and 53.9. Based on the angles obtained, these structures are predicted to be waves which are generally associated with turbulent spots during the transition process.

7. Acknowledgement

This work has been supported by the Air Force Office of Scientific Research through grant FA9550-16-1-0076.

References

Agrawal, R., Whalley, R. D., Ng, H. C.-H., Dennis, D. J. C., & Poole, R. J. (2019). Minimizing recalibration using a non-linear regression technique for thermal anemometry. *Exp. Fluids*, *60*, 116.

Aida, H., Tsukahara, T., & Kawaguchi, Y. (2010). DNS of turbulent spot developing into turbulent stripe in plane Poiseuille flow. *In Proceedings of ASME 2010 3rd Joint US–European Fluids Engineering Summer Meeting*, (p. 2125–2130).

Aida, H., Tsukahara, T., & Kawaguchi, Y. (2014). Development of a turbulent spot into a stripe pattern in plane Poiseuille flow. *arXiv:1410.0098 [physics.flu-dyn]*, .

Alavyoon, F., Henningson, D. S., & Alfredsson, P. H. (1986). Turbulent spots in plane Poiseuille flow–flow visualization. *Phys. Fluids*, *29*, 1328–1331.

Alfredsson, P. H., Johansson, A. V., Haritonidis, J. H., & Eckelmann, H. (1988). The fluctuating wall-shear stress and the velocity field in the viscous sublayer. *Phys. Fluids*, *31*, 1026–1033.

Brethouwer, G., Duguet, Y., & Schlatter, P. (2012). Turbulent–laminar coexistence in wall flows with coriolis, buoyancy or lorentz forces. *Journal of Fluid Mechanics*, *704*, 137–172.

Carlson, D. R., Widnall, S. E., & Peeters, M. F. (1982). A flow-visualization study of transition in plane Poiseuille flow. *J. Fluid Mech.*, *121*, 487–505.

Chantry, M., Tuckerman, L. S., & Barkley, D. (2017). Universal continuous transition to turbulence in a planar shear flow. *Journal of Fluid Mechanics*, *824*.

Davies, S. J., & White, C. M. (1928). An experimental study of the flow of water in pipes of rectangular section. *Proc. R. Soc. London, Ser. A*, *119*, 92–107.

Dean, R. (1978). Reynolds number dependence of skin friction and other bulk flow variables in two-dimensional rectangular duct flow. *ASME. J. Fluids Eng.*, *100*, 215–223.

Durst, F., Ray, S., Ünsal, B., & Bayoumi, O. (2005). The development lengths of laminar pipe and channel flows. *ASME. J. Fluids Eng.*, *127*, 1154–1160.

Gubian, P.-A., Stoker, J., Medvescek, J., Mydlarski, L., & Baliga, B. R. (2019). Evolution of wall shear stress with reynolds number in fully developed turbulent channel flow experiments. *Phys. Rev. Fluids*, *4*, 074606.

Henkel, M., Hinrichsen, H., Lübeck, S., & Pleimling, M. (2008). *Non-equilibrium phase transitions* volume 1. Springer.

Hinrichsen, H. (2000). Non-equilibrium critical phenomena and phase transitions into absorbing states. *Advances in physics*, *49*, 815–958.

Hu, Z., Morfey, C. L., & Sandham, N. D. (2006). Wall pressure and shear stress spectra from direct simulations of channel flow. *AIAA Journal*, *44*, 1541–1549.

Hutchins, N., Nickels, T. B., Marusic, I., & Chong, M. (2009). Hot-wire spatial resolution issues in wall-bounded turbulence. *Journal of Fluid Mechanics*, *635*, 103–136.

Jovanović, J., Durst, F., & Johansson, T. (1993). Statistical analysis of the dynamic equations for higher-order moments in turbulent wall bounded flows. *Phys. Fluids A: Fluid Dynamics*, *5*, 2886–2900.

Kao, T. W., & Park, C. (1970). Experimental investigations of the stability of channel flows. Part 1. Flow of a single liquid in a rectangular channel. *J. Fluid Mech.*, *43*, 145–164.

Keirsbulck, L., Labraga, L., & el Hak, M. G. (2012). Statistical properties of wall shear stress fluctuations in turbulent channel flows. *Int. J. Heat Fluid Flow*, *37*, 1 – 8.

Kline, S., & McClintock, F. (1953). Describing uncertainties in single-sample experiments. *Mechanical Engineering*, *75*, 3–8.

Krogstad, P.-Å., Kaspersen, J., & Rimestad, S. (1998). Convection velocities in a turbulent boundary layer. *Phys. Fluids*, *10*, 949–957.

Kushwaha, A., Park, J. S., & Graham, M. D. (2017). Temporal and spatial intermittencies within channel flow turbulence near transition. *Phys. Rev. Fluids*, *2*, 024603.

Lemoult, G., Aider, J.-L., & Wesfreid, J. E. (2013). Turbulent spots in a channel: large-scale flow and self-sustainability. *J. Fluid Mech.*, *731*, R1. doi:`10.1017/jfm.2013.388`.

Lemoult, G., Shi, L., Avila, K., Jalikop, S. V., Avila, M., & Hof, B. (2016). Directed percolation phase transition to sustained turbulence in couette flow. *Nature Physics*, *12*, 254–258.

Li, F., & Widnall, S. E. (1989). Wave patterns in plane poiseuille flow created by concentrated disturbances. *Journal of Fluid Mechanics*, *208*, 639–656.

Lien, K., Monty, J., Chong, M., & Ooi, A. (2004). The entrance length for fully developed turbulent channel flow. *15th Australasian Fluid Mechanics Conference (Sydney, Australia)*, .

Marusic, I., Mathis, R., & Hutchins, N. (2010). Predictive model for wall-bounded turbulent flow. *Science*, *329*, 193–196.

Nishioka, M., A, S. I., & Ichikawa, Y. (1975). An experimental investigation of the stability of plane Poiseuille flow. *J. Fluid Mech.*, *72*, 731–751.

Orlu, R., & Schlatter, P. (2011). On the fluctuating wall-shear stress in zero pressure-gradient turbulent boundary layer flows. *Phys. Fluids*, *23(2)*.

Orszag, S. A. (1971). Accurate solution of the Orr–Sommerfeld stability equation. *J. Fluid Mech.*, *50*, 689–703. doi:`10.1017/S0022112071002842`.

Patel, V. C., & Head, M. R. (1969). Some observations on skin friction and velocity profiles in fully developed pipe and channel flows. *J. Fluid Mech.*, *38*, 181–201.

Pomeau, Y. (1986). Front motion, metastability and subcritical bifurcations in hydrodynamics. *Physica D: Nonlinear Phenomena*, *23*, 3 – 11.

Pope, S. B. (2000). *Turbulent Flows*. Cambridge University Press.

Reynolds, O. (1883). Xxix. an experimental investigation of the circumstances which determine whether the motion of water shall be direct or sinuous, and of the law of resistance in parallel channels. *Philosophical Transactions of the Royal society of London*, (pp. 935–982).

Sano, M., & Tamai, K. (2016). A universal transition to turbulence in channel flow. *Nature Physics*, *12*, 249–253.

Seki, D., & Matsubara, M. (2012). Experimental investigation of relaminarizing and transitional channel flows. *Phys. Fluids*, *24*, 124102.

Takeishi, K., Kawahara, G., Wakabayashi, H., Uhlmann, M., & Pinelli, A. (2015). Localized turbulence structures in transitional rectangular-duct flow. *J. Fluid Mech.*, *782*, 368–379.

Takeuchi, K. A., Kuroda, M., Chaté, H., & Sano, M. (2007). Directed percolation criticality in turbulent liquid crystals. *Physical review letters*, *99*, 234503.

Tao, J., Eckhardt, B., & Xiong, X. (2018). Extended localized structures and the onset of turbulence in channel flow. *Physical Review Fluids*, *3*, 011902.

Tatsumi, T., & Yoshimura, T. (1990). Stability of the laminar flow in a rectangular duct. *J. Fluid Mech.*, *212*, 437–449.

Tsukahara, T., Kawaguchi, Y., & Kawamura, H. (2014). An experimental study on turbulent-stripe structure in transitional channel flow. *arXiv:1406.1378 [physics.flu-dyn]*, .

Tsukahara, T., Seki, Y., Kawamura, H., & Tochio, D. (2005). DNS of turbulent channel flow at very low reynolds numbers. *Proceedings of the 4th international symposium on turbulence and shear flow phenomena, Williamsburg, USA*, (p. 935–40).

Tuckerman, L. S., Kreilos, T., Schrobsdorff, H., Schneider, T. M., & Gibson, J. F. (2014). Turbulent-laminar patterns in plane poiseuille flow. *Physics of Fluids*, *26*, 114103.

Vinuesa, R., Schlatter, P., & Nagib, H. M. (2015). Characterization of the secondary flow in turbulent rectangular ducts with varying aspect ratio. *Proceedings of the 9th International Symposium on Turbulence and Shear Flow Phenomena, Melbourne, Australia*, (p. 1–6).

Whalley, R., Dennis, D., Graham, M., & Poole, R. (2019). An experimental investigation into spatiotemporal intermittencies in turbulent channel flow close to transition. *Experiments in Fluids*, *60*, 102.

Whalley, R. D., Park, J. S., Kushwaha, A., Dennis, D. J. C., Graham, M. D., & Poole, R. J. (2017). Low-drag events in transitional wall-bounded turbulence. *Phys. Rev. Fluids*, *2*, 034602.

Wygnanski, I., Sokolov, M., & Friedman, D. (1975). On transition in a pipe. part 2. the equilibrium puff. *Journal of Fluid Mechanics*, *69*, 283–304.

Wygnanski, I. J., & Champagne, F. (1973). On transition in a pipe. part 1. the origin of puffs and slugs and the flow in a turbulent slug. *Journal of Fluid Mechanics*, *59*, 281–335.

Xiao, X., & Song, B. (2019). The growth mechanism of turbulent bands in channel flow at low reynolds numbers. *arXiv preprint arXiv:1910.12254*, .

Xiong, X., Tao, J., Chen, S., & Brandt, L. (2015). Turbulent bands in plane-Poiseuille flow at moderate Reynolds numbers. *Phys. Fluids*, *27*, 041702.